

ARTICLE

Open Access

Tuning the density of zero-field skyrmions and imaging the spin configuration in a two-dimensional Fe_3GeTe_2 magnet

Bei Ding¹, Xue Li^{1,2}, Zefang Li^{1,2}, Xuekui Xi¹, Yuan Yao¹ and Wenhong Wang³

Abstract

With the advent of ferromagnetism, two-dimensional (2D) van der Waals (vdW) magnets have attracted particular attention in exploring topological spin textures, such as skyrmions used for next-generation spintronic devices. The discovery of magnetic skyrmions in Fe_3GeTe_2 (FGT) has sparked interest in investigating the spin configurations of skyrmions in FGT. Here, we used an in situ Lorentz microscope to directly demonstrate the generation and sustainability of Bloch-type skyrmions in a zero magnetic field over a wide temperature range in 2D vdW FGT. By tuning the value of the external magnetic field, the highest-density hexagonal skyrmion lattice emerges after reducing the magnetic field to zero. Moreover, by tilting the FGT nanosheet, we found that the field-free Bloch-type skyrmions in FGT can also represent an invisible contrast when the tilt angle is zero, but a reversed magnetic contrast emerges at a high tilt angle. On the basis of our experiments, we discuss the possible mechanisms for such variable magnetic contrast. These findings offer valuable insights into the spin configurations of skyrmions in 2D vdW FGT and shed light on the identification of spin configurations via Lorentz microscopy.

Introduction

Two-dimensional van der Waals (2D vdW) materials with long-range ferromagnetic orders presenting diverse novel phenomena^{1–5} show promise for fundamental physics and device applications^{6,7}. Among these materials, Fe_3GeTe_2 (FGT) has drawn particular attention due to its strong perpendicular magnetic anisotropy and long-range ferromagnetic order ranging from bulk crystals down to monolayers^{8–11}. More importantly, the Curie temperature (T_C) of FGT atomic layers is controllable via electrostatic gating or patterned microstructures^{12,13}. In conjunction with these novel properties, magnetic domain structures have been recently investigated in 2D vdW FGT. Complex magnetic domain structures, including labyrinthine domain structures¹⁰, bubble domains¹⁴, double-walled domains¹⁵, and spike-like domains¹⁶, have been observed

via magnetic force microscopy. Recent investigations of FGT via Lorentz transmission electron microscopy (LTEM) with the application of a magnetic field have led to the discovery of skyrmions. The magnetic field and temperature play a crucial role in skyrmion generation and stability. Rapid cooling below T_C with a proper magnetic field has led to field-free skyrmions being observed not only in non-centrosymmetric magnet FeGe ¹⁷ and MnSi ¹⁸ but also in centrosymmetric magnet MnNiGa ^{19,20}. Unfortunately, such thermal manipulations of skyrmions in 2D vdW magnets remain elusive. Meanwhile, these field-free skyrmions provide an easy way to identify the spin configurations of skyrmions regardless of the application of a magnetic field.

Very recently, Néel-type skyrmions supported by interfacial Dzyaloshinskii–Moriya interactions were discovered in FGT heterostructures^{21,22}. Simultaneously, Bloch-type skyrmions stabilized by magnetic dipole interactions have also been reported in FGT nanosheets²³. As theoretically predicted, Bloch-type magnetic twists

Correspondence: Wenhong Wang (wenhongwang@tiangong.edu.cn)

¹Institute of Physics, Chinese Academy of Sciences, Beijing 100190, China

²University of Chinese Academy of Sciences, Beijing 100049, China

Full list of author information is available at the end of the article

© The Author(s) 2022



Open Access This article is licensed under a Creative Commons Attribution 4.0 International License, which permits use, sharing, adaptation, distribution and reproduction in any medium or format, as long as you give appropriate credit to the original author(s) and the source, provide a link to the Creative Commons license, and indicate if changes were made. The images or other third party material in this article are included in the article's Creative Commons license, unless indicated otherwise in a credit line to the material. If material is not included in the article's Creative Commons license and your intended use is not permitted by statutory regulation or exceeds the permitted use, you will need to obtain permission directly from the copyright holder. To view a copy of this license, visit <http://creativecommons.org/licenses/by/4.0/>.

usually emerge in centrosymmetric magnets with competition between dipole interactions and uniaxial magnetic anisotropy, as reported in Mn-Ni-Ga²⁴, Ni₂MnGa²⁵, Fe₃Sn₂²⁶, and 2D vdW Cr₂Ge₂Te₆²⁷. In centrosymmetric FGT with a space group of P63/mmc, Néel-type skyrmions in previous reports seem to be a subject of controversy. Thus, direct identification of the spin configurations of skyrmions in 2D vdW FGT deserves further investigation.

In this work, the generation and sustainability of Bloch-type skyrmions in a zero magnetic field over a wide temperature range in 2D vdW FGT were directly demonstrated via LTEM. By tuning the value of the external magnetic field, the highest-density hexagonal skyrmion lattice emerges after reducing the magnetic field to zero. Micromagnetic simulation reveals that compared with stripe domains, the highest-density skyrmion lattice has stronger total energy, indicating that it is in a metastable state. In addition, we found that the field-free Bloch-type skyrmions in FGT can also exhibit no contrast when the tilt angle is zero but present a reversed magnetic contrast at a high tilt angle. On the basis of our experiments, we discuss the possible mechanisms for this disappearing magnetic contrast.

Materials and methods

Sample synthesis

High-quality Fe₃GeTe₂ single crystals were grown using the Te self-flux method from a mixture of pure elements Fe (99.99%), Ge (99.9999%), and Te (99.995%) with a composition of Fe₂GeTe₄²⁸. The mixture was then sealed in an evacuated quartz tube and heated to 1000 °C. The melt was held at 1000 °C for 3 h and then cooled slowly to 680 °C at a rate of 1 °C/h, and the excess Te flux was removed by spinning the tube. The typical size of the single crystals was ~5 × 5 × 0.2 mm, with a cleavable layer in the *ab* plane. The composition of the single-crystal FGT was further checked by scanning energy dispersive X-ray spectroscopy, confirming that the atomic ratio was ~3:1:2 (Fig. S1).

Lorentz TEM measurement

The nanosheets for Lorentz TEM observation were fabricated from a single crystal by using a focused iron beam. The magnetic domain was directly observed by using a Tecnai F20 in Lorentz TEM mode and a JEOL 2100F Lorentz TEM, both equipped with liquid nitrogen and low-temperature holders (~90 K) to study the temperature dependence of the magnetic textures. The objective lens was turned off when the sample holder was inserted, and the perpendicular magnetic field was induced to the nanosheet by increasing the objective lens in a small increment. For tilting experiments, the crystalline orientation of the nanosheets was first checked by

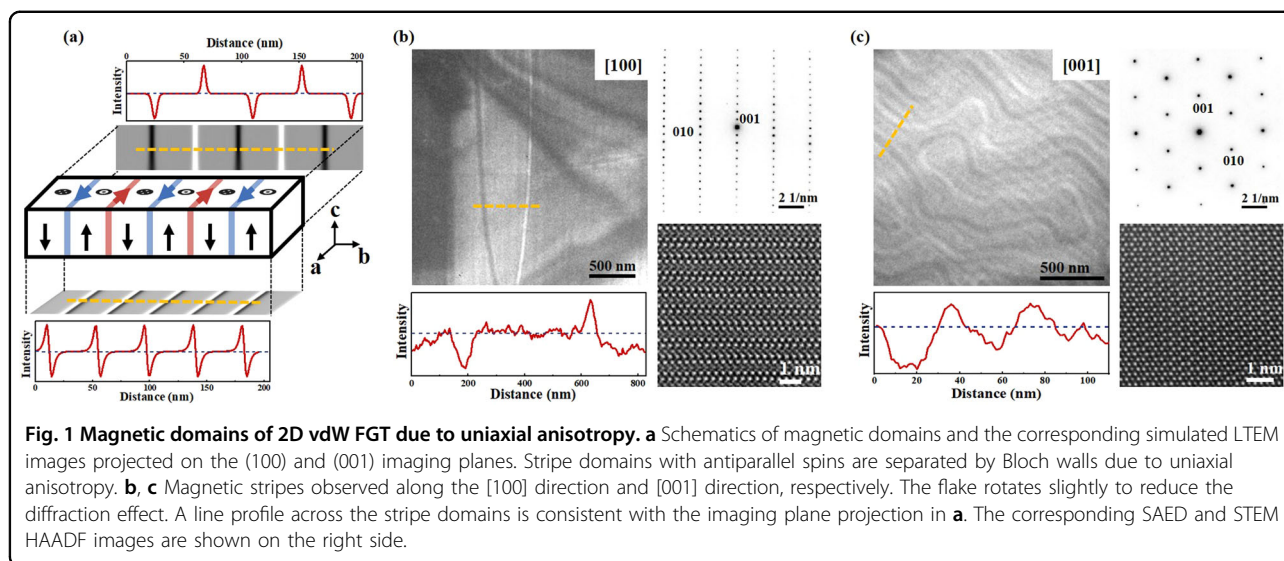
selected-area electron diffraction (SAED) to ensure compliance along the [001] direction. After marking the value of this angle, a series of tilting experiments were performed. In addition, the specific field cooling (FC) manipulation is shown as follows. First, the sample was heated higher than the Curie temperature $T_C \sim 150$ K. Second, the perpendicular magnetic field was applied by increasing the objective lens current gradually in a very small increment. Third, the temperature of the sample was cooled gradually from 150 K to 93 K. Finally, at 93 K, the small perpendicular magnetic field was turned off.

Micromagnetic simulations

Micromagnetic simulation was performed via the Object Oriented MicroMagnetic Framework (OOMMF) code based on the LLG function²⁹. The slab was 2000 × 2000 × 100 nm with a rectangular mesh of size 5 × 5 × 5 nm. The saturation magnetization was chosen as $M_s = 2.23 \times 10^5$ A/m at 100 K, and the magnetic anisotropy constant K_u was 0.5×10^5 J/m³. To make analytic progress, we considered an initially random spin state as the paramagnetic state. A field cooling procedure was performed as follows. Initially, the slab was set as a random state, and an external field was applied along the *z*-axis. After that, the perpendicular field was reduced to zero, and the slab was relaxed to an equilibrium state with each step of 30 ns.

Results

The 2D vdW FGT is a ferromagnet with a strong uniaxial magnetic anisotropy and an easy axis along the *c*-axis, while it exhibits absolute isotropic characteristics in the *ab* plane³⁰. Owing to competition between the uniaxial magnetic anisotropy and magnetic dipole interaction, stripe domains separated by Bloch walls spontaneously stabilized without an external magnetic field, as schematically shown in Fig. 1a. In Fig. 1b, c, we show the magnetic domain at 93 K along two orthogonal imaging directions. The corresponding crystalline orientation and crystal structure were examined by using SAED and scanning transmission electron microscopy with high-angle annular dark-field atomic resolution, which coincides with previous reports^{23,31}. In the case of the *bc* plane, the magnetic contrast induced by the spins inside the domain formed alternating dark or bright stripes, which were further identified by the line profile of magnetic contrast. For magnetic domains observed in the *ab* plane, the flake was tilted to reduce the diffraction contrast and induce magnetic contrast, which is similar to an approach reported in the previous work²³. Clearly, the LTEM contrast is only generated by the domain wall, resulting in bright–dark or dark–bright stripes, as verified by the line profile shown in Fig. 1c. The different magnetic domains in the two orthogonal imaging planes



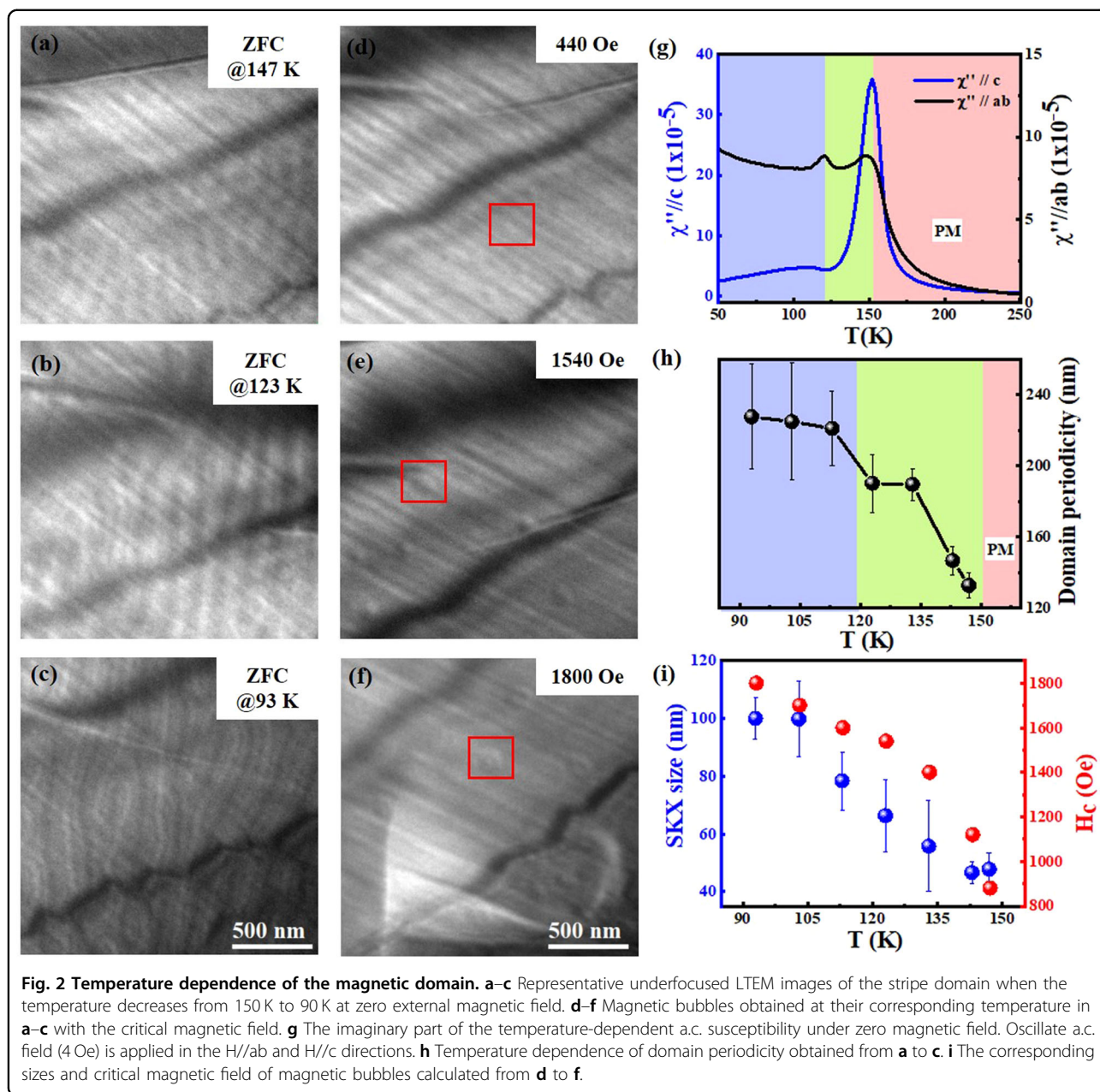
demonstrate that the strong magnetocrystalline anisotropy of FGT persists despite additional shape anisotropy terms arising in the cross-section TEM sample. It is noteworthy that with decreasing width of the domain wall, the magnetic contrast in the ab plane gradually vanished, which will be discussed later.

The evolution of the magnetic stripe as a function of temperature and magnetic field in the bc plane was studied in the Supporting Information (Fig. S2); here, we focus on the magnetic domain in the ab plane. The flake along the [001] direction was tilted to reduce the diffraction contrast and induce magnetic contrast. Figure 2a–c shows the magnetic domain as a function of temperature observed via LTEM under a zero field. As the temperature decreases to 147 K, slightly below $T_c \sim 150$ K, magnetic stripes emerge. Upon further cooling, the stripes become wider and more distinctive (Fig. S3). The period of the domain as a function of temperature is shown in Fig. 2h. With the application of an external magnetic field, the stripes gradually transformed into bubbles (details seen in Supporting Information, Fig. S4). In Fig. 2d–f, we show the temperature-dependent LTEM images of bubbles at temperatures ranging from 147 K to 93 K under their corresponding critical magnetic field. Clearly, the critical magnetic field increases with decreasing temperature (Fig. S5). Simultaneously, the size of bubbles represents a similar variation, as shown in Fig. 2i. The magnetic domain texture is further analyzed with magnetic properties in FGT, as shown in Fig. 2g. The a.c. susceptibility measurements in the $H//c$ and $H//ab$ directions were performed to identify the magnetic transition. For the 150 K transition, the peak in each direction appears, which is related to the Curie temperature. In contrast, at the 118 K transition, the peak only appears in the black curve (in the ab plane) but remains almost absent in the $H//c$ direction.

Interestingly, the period of the magnetic stripe exactly represents a significant change above 118 K and gradually remains constant at lower temperatures. The varied periodicity may result from the pinned magnetic domain wall³² or a spin-flop transition¹⁴, which needs further investigation.

To obtain a field-free skyrmion lattice with the highest density, we tuned the magnitude of the cooling field (H_{CF}), as shown in Fig. 3a–c. The detailed cooling procedure and specific LTEM images are shown in the Methods and Fig. S6. When the magnetic field is lower than 100 Oe or higher than 700 Oe, a stripe emerges. With the magnetic field increasing from 100 Oe to 700 Oe, the size of skyrmions first decreases and then increases (Fig. 3g). Meanwhile, the density of skyrmions represents an inverse variation reaching a maximum value at $H_{CF} \sim 400$ Oe (Fig. 3b). A stronger magnetic field will force nucleation sites to agglomerate, thereby reducing skyrmion density and enlarging skyrmion size. Clearly, the skyrmion density is apparently enhanced via FC manipulation compared with the random distribution induced solely by the magnetic field. In addition, the spin configuration of field-free skyrmions is further analyzed, which represents dark to bright or bright to dark rings in the underfocused images identified with Bloch-type domain walls separating the spin-up and spin-down domains²³.

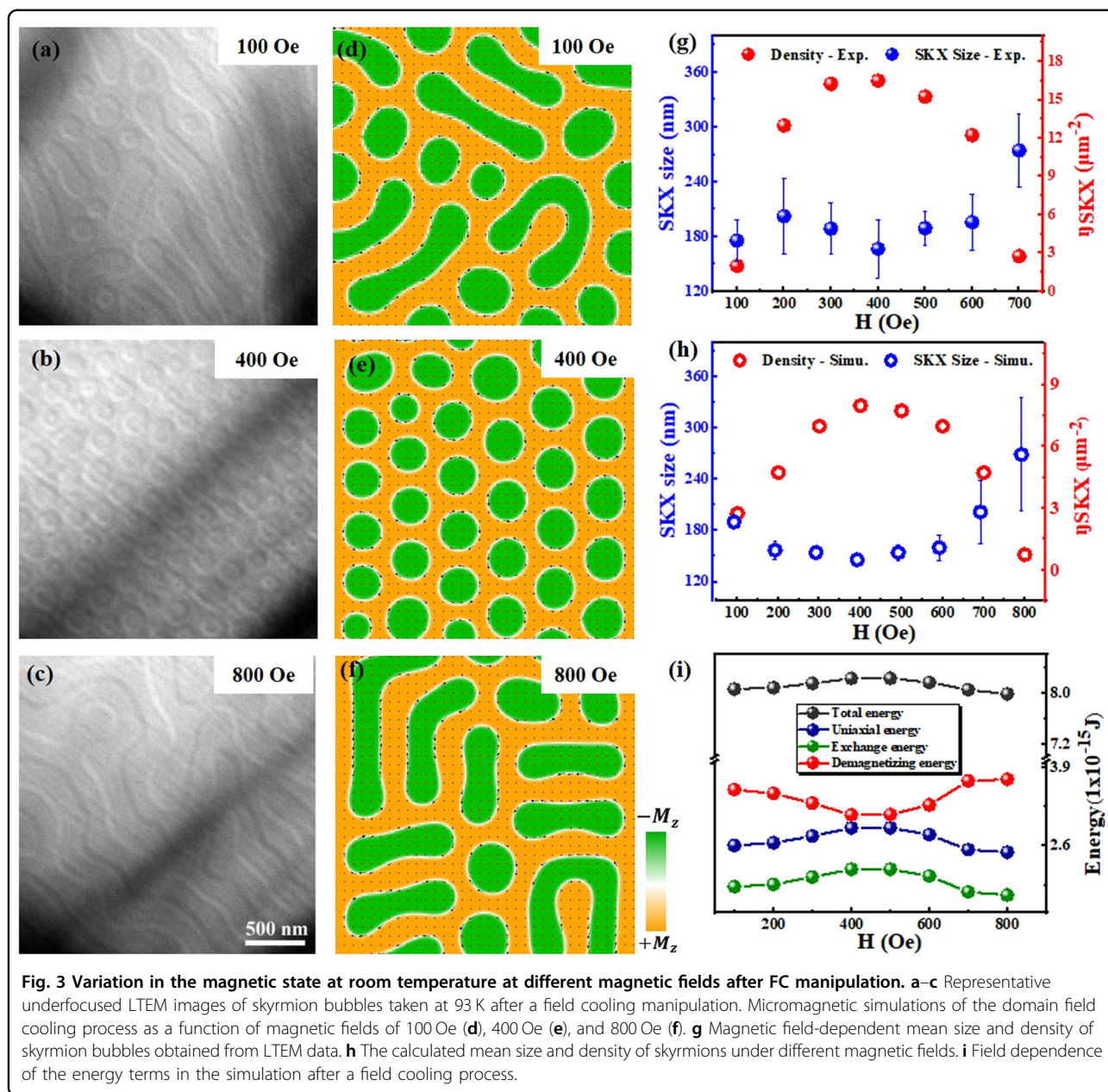
To understand the mechanism stabilizing the skyrmion lattice after field cooling, we performed micromagnetic simulation via the OOMMF code. The input magnetic parameters were used as reported in previous work²³. In this approach, we take a random spin configuration as the paramagnetic state. Figure 3d–f shows the representative remanent state after the field-cooling manipulation. The variation in the size and density of the skyrmions is the same as that observed in the LTEM experiments, as



shown in Fig. 3h. At $H_{CF} = 400$ Oe, the skyrmions with a homogeneous circular shape are closely packed, forming hexagonal lattice skyrmions. As the magnetic field varies, individual skyrmions stretch to deform the lattice arrangement. The corresponding formation of these spin configurations in centrosymmetric magnets should originate from the competition of the exchange energy, the magnetic anisotropy energy, and the demagnetizing energy, as shown in Fig. 3i. As the external magnetic field increases, the strength of the dipole interaction exhibits a reversal variation compared with the other two interactions, reaching a minimum value at $H_{CF} = 400$ Oe. Owing to the high density of skyrmions, an increasing number of

domain walls reduces the demagnetizing energy; however, it simultaneously gives rise to the exchange energy. Meanwhile, various magnetic moments deviate from the easy axis, resulting in an increasing uniaxial magneto-crystalline anisotropy. The magnetic field-dependent total energy is obtained; obviously, it represents a maximum value with the highest density of skyrmions, which indicates that, compared with the stripe domain, the thermal-equilibrium skyrmion lattice is in a metastable state.

Figure 4 represents the externally applied temperature (T)–magnetic field (H) phase diagram with the ZFC process and FC process measured by systematic Lorentz TEM observations at various T and B . The formation and



annihilation magnetic field for skyrmions are plotted by white dashed lines. As shown in Fig. 4a, the phase diagram for skyrmions is limited. The magnetic field to generate skyrmions increases with decreasing temperature. After FC manipulation, the high-density yellow-colored area with zero-field skyrmions covers the entire temperature range toward T_C , as shown in Fig. 4b.

On the basis of field-free skyrmions, we further investigate the spin configuration observed in the FGT flake at various oblique angles, as shown in Fig. 5. The parameter α is defined as the angle between the electron beam direction and the [001] direction of the flake. Based on the direct LTEM observation, at a zero-degree tilt, no

magnetic contrast appeared in the defocused LTEM image. With increasing oblique angles, the magnetic contrast gradually appeared. At $\alpha = 7^\circ$, the sharp contrast of dark to bright or bright to dark rings in the images identified with Bloch domain walls, which is further demonstrated by the line scan positions for contrast profiles of a single skyrmion with two peaks clearly observed in the bottom of Fig. 5b. At a higher tilting angle $\sim \pm 20^\circ$, the skyrmion represents half-black/half-white magnetic contrast and a reversal contrast with reversing tilting direction. This can be easily distinguished from the contrast profile. Clearly, only one peak was observed at a high tilted angle ($\pm 20^\circ$), and the intensity of the profile

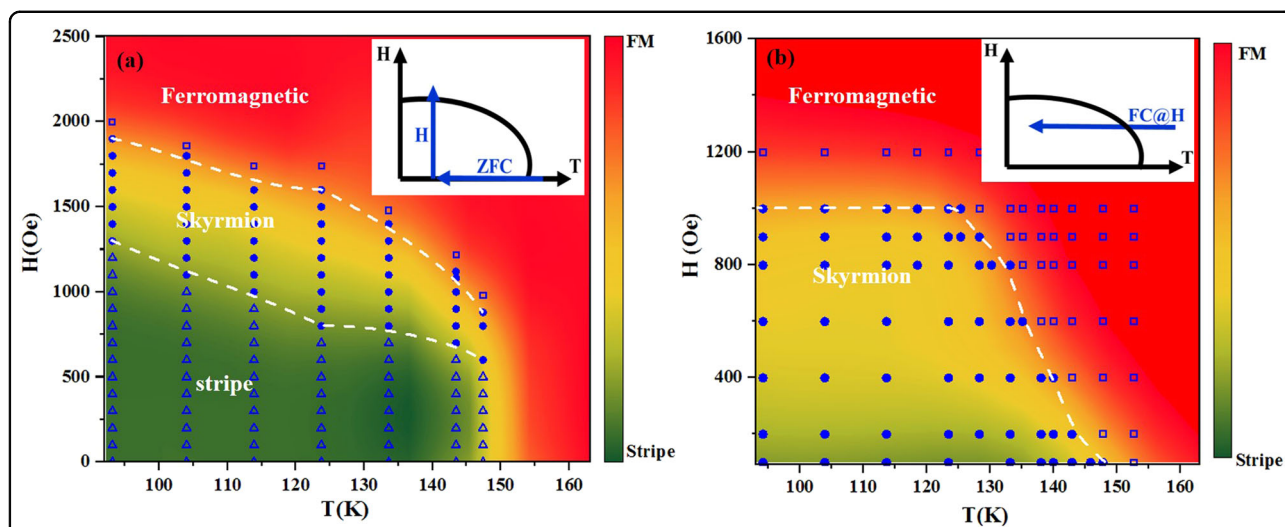


Fig. 4 Experimental phase map of the magnetic domain as a function of magnetic field and temperature based on the LTEM observation. **a** The flake was cooled to a specific temperature, and then an external magnetic field was applied. **b** An external magnetic field was applied and then slowly cooled down. The points represent different magnetic states: hollow triangle - stripe, dot - skymion and hollow rectangle - ferromagnetic state.

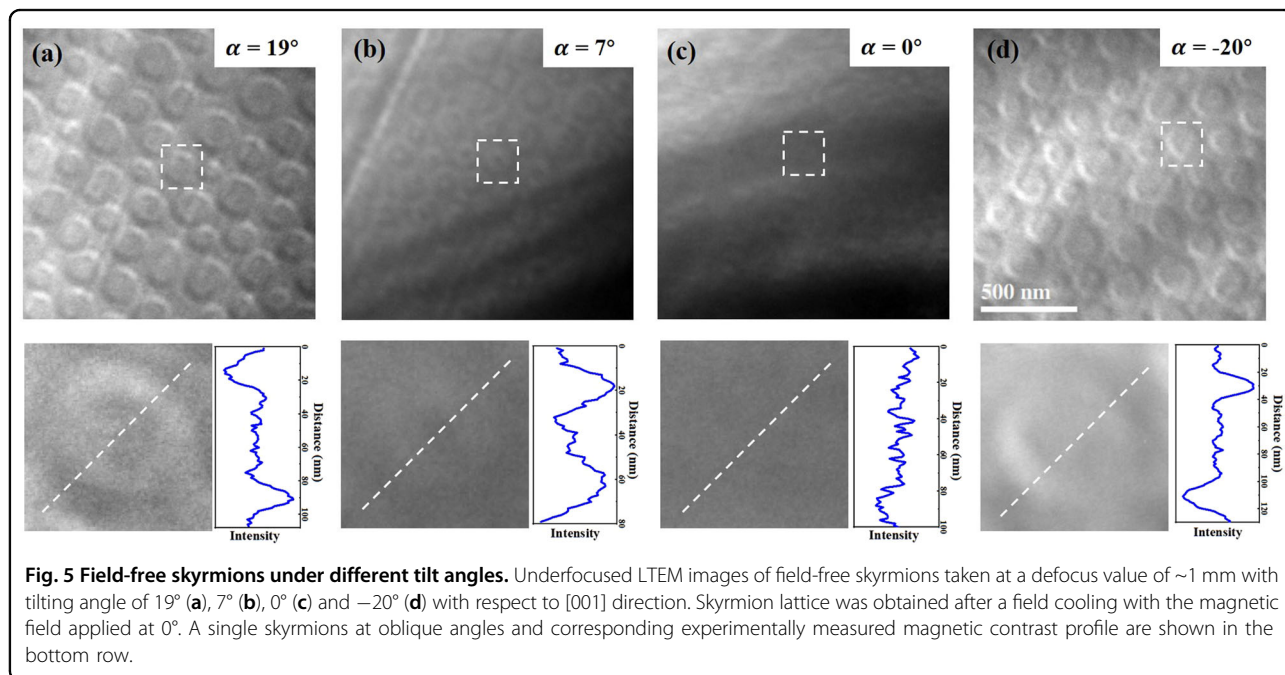


Fig. 5 Field-free skyrmions under different tilt angles. Underfocused LTEM images of field-free skyrmions taken at a defocus value of ~ 1 nm with tilting angle of 19° (a), 7° (b), 0° (c) and -20° (d) with respect to [001] direction. Skyrmion lattice was obtained after a field cooling with the magnetic field applied at 0° . A single skyrmions at oblique angles and corresponding experimentally measured magnetic contrast profile are shown in the bottom row.

represents mirror symmetry with a reversing tilting angle. The same experiment was performed on the magnetic stripe domain, as shown in Fig. S7.

Discussion

We now discuss the possibility that leads to the varied observations of magnetic contrast in the FGT thin plate. LTEM is sensitive to the in-plane magnetic component,

which further induces the phase shift of the electron beam. Note that magnetic contrast was not observed at the zero tilt because of the symmetric deflection of magnetic texture, such as in a Néel type skyrmion^{33,34}, which can result from a small magnetization³⁵ or a narrow domain wall³⁶ of a Bloch-type twist. Based on the above observation, we exclude the existence of a Néel-type magnetic domain in the FGT flake. Through

magnetization curve measurements, the saturation magnetization of FGT is calculated to be 0.275 T (100 K), which is approximately 3.6 times smaller than that in Mn-Ni-Ga (300 K). Such small magnetization makes it difficult to detect the magnetic contrast.

Another possible reason can be induced from a very thin domain wall, too narrow to be detected by LTEM, which has been reported in a uniaxial centrosymmetric crystal $\text{La}_{1.2}\text{Sr}_{1.8}(\text{Mn}_{1-y}\text{Ru}_y)_2\text{O}_7$ with Bloch-type bubbles³⁶. For a 2D vdW FGT, as shown in Fig. 1a, the magnetic contrast in the *ab* plane is only generated by the domain wall. With a large magnetic anisotropy ratio $Q = K_u/K_d = 16.4 \gg 1$ (K_u is defined as the uniaxial anisotropy coefficient, while K_d is the stray field energy coefficient), the thickness of the domain wall was estimated as 2.5 nm¹⁶. Accompanied by the crystalline diffraction contrast along the [001] direction, it becomes more difficult to observe such a thin magnetic domain. However, when the flake was slightly tilted to reduce diffraction contrast, the magnetization component of the domain wall perpendicular to the beam path caused Lorentz deflection, leading to a visible magnetic domain texture. However, a large defocus value (~1 mm) was still used to make the magnetic contrast distinguishable due to a small magnetization. With a higher tilt angle ($\alpha = \pm 20^\circ$) (Fig. 5a, d), the in-plane components of the core and peripheral out-of-plane spins mainly contribute to inducing magnetic contrast. When we reverse the tilting direction, the in-plane components of spins also reverse their direction, thus resulting in an opposite magnetic contrast. Notably, our previous observation of the magnetic domain in FGT was also performed at a small tilt angle, which was not mentioned in the previous work. To date, tilting samples via LTEM is considered evidence for the identification of Bloch- or Néel-type magnetic structures. For the Néel-type magnetic structure, the LTEM images represent no magnetic contrast at zero tilting. A similar phenomenon may exist in Bloch-type magnetic twisting inside a thin domain wall. In this case, the magnetic texture in FGT deserves further investigation via a three-dimensional (3D) electron tomography technique or LTEM observation assisted by an in-plane magnetic field³⁷.

Conclusions

In summary, a controllable cooling field-induced field-free skyrmion was investigated in 2D vdW FGT. An appropriate cooling field exists to generate the highest-density skyrmions, which indicates that the magnetic field plays a crucial role in the generation of skyrmions. Theoretical simulations have demonstrated that the field-free skyrmion lattice is in a metastable state. We also examined the stability of the skyrmion lattice in FGT over a wide range of temperatures and magnetic fields, including its zero-field manifestation. On the other hand, we found

that field-free Bloch-type skyrmions in FGT can also represent no contrast when the tilt angle is zero, which results from the thin domain wall. Our results can support a further understanding of the spin configuration of skyrmions in 2D vdW materials.

Acknowledgements

This work is supported by the National Natural Science Foundation of China (Nos. 11974406 and 11874410), the Strategic Priority Research Program (B) of the Chinese Academy of Sciences (CAS) (XDB33000000), and the China Postdoctoral Science Foundation (No. 2021M693365). We thank Ying Zhang for assistance with LTEM experiments.

Author details

¹Institute of Physics, Chinese Academy of Sciences, Beijing 100190, China. ²University of Chinese Academy of Sciences, Beijing 100049, China. ³Tiangong University, Tianjin 300387, China

Author contributions

B.D. and W.H.W. proposed the idea and designed the experiments. The single crystal was synthesized by X.L. and Z.F.L. B.D. prepared the lamella, performed the Lorentz-TEM measurement, and analyzed the data. Y.Y. and X.K.X. contributed to the data analysis. All authors discussed the paper; B.D. and W.H.W. prepared the manuscript with input from all authors.

Conflict of interest

The authors declare no competing interests.

Publisher's note

Springer Nature remains neutral with regard to jurisdictional claims in published maps and institutional affiliations.

Supplementary information The online version contains supplementary material available at <https://doi.org/10.1038/s41427-022-00418-z>.

Received: 29 January 2022 Revised: 28 June 2022 Accepted: 7 July 2022
Published online: 2 September 2022

References

- Kim, K. et al. Large anomalous Hall current induced by topological nodal lines in a ferromagnetic van der Waals semimetal. *Nat. Mater.* **17**, 794–799 (2018).
- You, Y. et al. Angular dependence of the topological Hall effect in the uniaxial van der Waals ferromagnet Fe_3GeTe_2 . *Phys. Rev. B* **100**, 134441 (2019).
- Zhang, Y. et al. Emergence of Kondo lattice behavior in a van der Waals itinerant ferromagnet, Fe_3GeTe_2 . *Sci. Adv.* **4**, eaao6791 (2018).
- Zhuang, H. L., Kent, P. R. C. & Hennig, R. G. Strong anisotropy and magnetostriction in the two-dimensional Stoner ferromagnet Fe_3GeTe_2 . *Phys. Rev. B* **93**, 134407 (2016).
- Song, T. et al. Giant tunneling magnetoresistance in spin-filter van der Waals heterostructures. *Science* **360**, 1214–1218 (2018).
- Huang, B. et al. Layer-dependent ferromagnetism in a van der Waals crystal down to the monolayer limit. *Nature* **546**, 270–273 (2017).
- Klein, D. R. et al. Probing magnetism in 2D van der Waals crystalline insulators via electron tunneling. *Science* **360**, 1218–1222 (2018).
- Deiseroth, H.-J., Aleksandrov, K., Reiner, C., Kienle, L. & Kremer, R. K. Fe_3GeTe_2 and Ni_3GeTe_2 —two new layered transition-metal compounds: crystal structures, HRTEM investigations, and magnetic and electrical properties. *Eur. J. Inorg. Chem.* **2006**, 1561–1567 (2006).
- Chen, B. et al. Magnetic properties of layered itinerant electron ferromagnet Fe_3GeTe_2 . *J. Phys. Soc. Jpn.* **82**, 124711 (2013).
- Fei, Z. et al. Two-dimensional itinerant ferromagnetism in atomically thin Fe_3GeTe_2 . *Nat. Mater.* **17**, 778–782 (2018).
- Wang, X. et al. Current-driven magnetization switching in a van der Waals ferromagnet Fe_3GeTe_2 . *Sci. Adv.* **5**, eaaw8904 (2019).
- Deng, Y. et al. Gate-tunable room-temperature ferromagnetism in two-dimensional Fe_3GeTe_2 . *Nature* **563**, 94–99 (2018).

13. Li, Q. et al. Patterning-induced ferromagnetism of Fe_3GeTe_2 van der Waals materials beyond room temperature. *Nano Lett.* **18**, 5974–5980 (2018).
14. Yi, J. et al. Competing antiferromagnetism in a quasi-2D itinerant ferromagnet: Fe_3GeTe_2 . *2D Mater.* **4**, 011005 (2016).
15. Nguyen, G. D. et al. Visualization and manipulation of magnetic domains in the quasi-two-dimensional material Fe_3GeTe_2 . *Phys. Rev. B* **97**, <https://doi.org/10.1103/PhysRevB.97.014425> (2018).
16. León-Brito, N., Bauer, E. D., Ronning, F., Thompson, J. D. & Movshovich, R. Magnetic microstructure and magnetic properties of uniaxial itinerant ferromagnet Fe_3GeTe_2 . *J. Appl. Phys.* **120**, <https://doi.org/10.1063/1.4961592> (2016).
17. Peng, L. et al. Relaxation dynamics of zero-field skyrmions over a wide temperature range. *Nano Lett.* **18**, 7777–7783 (2018).
18. Yu, X. et al. Aggregation and collapse dynamics of skyrmions in a non-equilibrium state. *Nat. Phys.* **14**, 832–836 (2018).
19. Ding, B. et al. Thermally induced generation and annihilation of magnetic chiral skyrmion bubbles and achiral bubbles in Mn–Ni–Ga magnets. *Appl. Phys. Lett.* **116**, <https://doi.org/10.1063/1.5142083> (2020).
20. Peng, L. et al. Real-space observation of nonvolatile zero-field skyrmion lattice generation in MnNiGa magnet. *Nano Lett.* <https://doi.org/10.1021/acs.nanolett.7b03792> (2017).
21. Wu, Y. et al. Néel-type skyrmion in $\text{WTe}_2/\text{Fe}_3\text{GeTe}_2$ van der Waals heterostructure. *Nat. Commun.* **11**, 3860 (2020).
22. Park, T.-E. et al. Néel-type skyrmions and their current-induced motion in van der Waals ferromagnet-based heterostructures. *Phys. Rev. B* **103**, <https://doi.org/10.1103/PhysRevB.103.104410> (2021).
23. Ding, B. et al. Observation of magnetic skyrmion bubbles in a van der Waals ferromagnet Fe_3GeTe_2 . *Nano Lett.* **20**, 868–873 (2020).
24. Ding, B. et al. Manipulating spin chirality of magnetic skyrmion bubbles by in-plane reversed magnetic fields in $(\text{Mn}_{1-x}\text{Ni}_x)_{65}\text{Ga}_{35}$ ($x = 0.45$) magnet. *Phys. Rev. Appl.* **12**, <https://doi.org/10.1103/PhysRevApplied.12.054060> (2019).
25. Phatak, C., Heinonen, O., De Graef, M. & Petford-Long, A. Nanoscale skyrmions in a nonchiral metallic multiferroic: Ni_2MnGa . *Nano Lett.* **16**, 4141–4148 (2016).
26. Hou, Z. et al. Observation of various and spontaneous magnetic skyrmionic bubbles at room temperature in a frustrated Kagome magnet with uniaxial magnetic anisotropy. *Adv. Mater.* **29**, <https://doi.org/10.1002/adma.201701144> (2017).
27. Han, M. G. et al. Topological magnetic-spin textures in two-dimensional van der Waals $\text{Cr}_2\text{Ge}_2\text{Te}_6$. *Nano Lett.* **19**, 7859–7865 (2019).
28. Liu, Y., Ivanovski, V. N. & Petrovic, C. Critical behavior of the van der Waals bonded ferromagnet Fe_3GeTe_2 . *Phys. Rev. B* **96**, 144429 (2017).
29. Donahue, M. J. & Donahue, M. OOMMF User's Guide, version 1.0. (1999).
30. Liu, W. et al. Field-dependent anisotropic magnetic coupling in layered ferromagnetic $\text{Fe}_{3-x}\text{GeTe}_2$. *Phys. Rev. B* **100**, <https://doi.org/10.1103/PhysRevB.100.104403> (2019).
31. Wang, H. et al. Characteristics and temperature-field-thickness evolutions of magnetic domain structures in van der Waals magnet Fe_3GeTe_2 nanolayers. *Appl. Phys. Lett.* **116**, 192403 (2020).
32. Tian, C.-K. et al. Domain wall pinning and hard magnetic phase in Co-doped bulk single crystalline Fe_3GeTe_2 . *Phys. Rev. B* **99**, <https://doi.org/10.1103/PhysRevB.99.184428> (2019).
33. Jiang, W. et al. Quantifying chiral exchange interaction for Néel-type skyrmions via Lorentz transmission electron microscopy. *Phys. Rev. B* **99**, <https://doi.org/10.1103/PhysRevB.99.104402> (2019).
34. Garlow, J. A. et al. Quantification of mixed Bloch–Néel topological spin textures stabilized by the Dzyaloshinskii–Moriya interaction in Co/Pd multilayers. *Phys. Rev. Lett.* **122**, 237201 (2019).
35. Sugawara, A. et al. Magnetic domain structure within half-metallic ferromagnetic kagome compound $\text{Co}_3\text{Sn}_2\text{S}_2$. *Phys. Rev. Mater.* **3**, <https://doi.org/10.1103/PhysRevMaterials.3.104421> (2019).
36. Morikawa, D. et al. Lorentz transmission electron microscopy on nanometric magnetic bubbles and skyrmions in bilayered manganites $\text{La}_{1.2}\text{Sr}_{1.8}(\text{Mn}_{1-y}\text{R}_y)_2\text{O}_7$ with controlled magnetic anisotropy. *Appl. Phys. Lett.* **107**, 212401 (2015).
37. Peng, L. et al. Tunable Néel–Bloch magnetic twists in Fe_3GeTe_2 with van der Waals structure. *Adv. Funct. Mater.* **31**, 2103583 (2021).